DEVELOPMENT AND ASSESSMENT OF THE BONE ALLOGRAFT-BASED MATERIAL FOR DLP 3D PRINTING

Bilyalov AR ✉, Chugunov SS, Akhatov ISh, Tikhonov AA, Shangina OR, Pavlov VN, Danilko KV, Galautdinov MF, Akbashev VN

Bashkir State Medical University, Ufa, Russia

The use of allogenic bone material as a ceramic filler for DLP printing makes it possible to obtain personalized complex-shaped implants combining the matrix biomimetic nature with the additive technology benefits. The study aimed to assess the possibility of using the calcined cortical bone allograft powder as part of photopolymerizable suspension for DLP printing and producing bioceramics with the characteristics comparable to that of synthetic hydroxyapatite by sintering. The bone allograft was subjected to multi-stage specialized treatment involving complete removal of cells with preservation of the intercellular matrix and collagen fiber structure. The calcined medical allograft was crushed, introduced into a photopolymerizable matrix, and used for DLP printing of the samples that were further sintered and analyzed by X-ray diffraction and energy-dispersive spectroscopy methods before and after additive production. The sintered material specific gravity was 81.5%, compressive strength — 75.8 MPa, tensile strength — 12 MPa, Young's modulus — 3.08 GPa, and Vickers hardness — 0.55 GPa, which was within the range of values for porous hydroxyapatite. After DLP printing and sintering the sample phase and elemental composition did not change considerably compared to the source calcined material. The calcined bone allograft powder is suitable for preparing photopolymerizable suspensions and subsequent DLP printing of ceramic samples without deteriorating the material phase and chemical stability. The resulting mechanical properties make it possible to consider this allogenic bone material as a promising candidate for production of personalized implants with sophisticated geometry.

Keywords: hydroxyapatite, 3D printing, bioceramics, allograft, alloplant, biomedical application, firing, ceramics

Funding: the study was supported by the Russian Science Foundation grant No. 23-15-20042.

Author contribution: Bilyalov AR, Chugunov SS — study planning, literature review, data interpretation, manuscript writing; Akhatov ISh — study planning, data interpretation, manuscript writing; Tikhonov AA — study planning, literature review, data acquisition, analysis, and interpretation; Shangina OR — study planning, data analysis and interpretation; Pavlov VN — study planning; Danilko KV — study planning, data acquisition, analysis, and interpretation; Galautdinov MF — data acquisition; Akbashev VN — literature review.

✉ **Correspondence should be addressed:** Azat R. Bilyalov
Lenina, 3, Ufa, 450008, Russia; azat.bilyalov@gmail.com

Received: 03.11.2025 **Accepted:** 29.11.2025 **Published online:** 18.12.2025

DOI: 10.24075/brsmu.2025.068

РАЗРАБОТКА И ИССЛЕДОВАНИЕ МАТЕРИАЛА НА ОСНОВЕ КОСТНОГО АЛЛОТРАНСПЛАНТАТА ДЛЯ DLP-3D-ПЕЧАТИ

А. Р. Билялов ✉, С. С. Чугунов, И. Ш. Ахатов, А. А. Тихонов, О. Р. Шангина, В. Н. Павлов, К. В. Данилко, М. Ф. Галаутдинов, В. Н. Акбашев

Башкирский государственный медицинский университет, Уфа, Россия

Использование аллогенного костного материала как керамического наполнителя для DLP-печати позволяет получать индивидуализированные имплантаты сложной формы, совмещающие биомиметичную природу матрицы с преимуществами аддитивных технологий. Целью работы было оценить возможность использования прокаленного порошка кортикального костного аллотрансплантата в составе фотополимеризуемой суспензии для DLP-печати и получения после спекания биокерамики с характеристиками, сопоставимыми с синтетическим гидроксиапатитом. Костный аллотрансплантат подвергали многоэтапной специализированной обработке с полным удалением клеток при сохранении структуры межклеточного матрикса и коллагеновых волокон. Прокаленный медицинский аллотрансплантат измельчали, вводили в фотополимеризуемую матрицу и использовали для DLP-печати образцов, которые затем спекали и анализировали методами рентгеновской дифракции и энергодисперсионной спектроскопии до и после аддитивного производства. Относительная плотность спеченного материала составила 81,5%, прочность на сжатие — 75,8 МПа, прочность на растяжение — 12 МПа, модуль Юнга — 3,08 ГПа и твердость по Виккерсу — 0,55 ГПа, что находится в диапазоне значений для пористого гидроксиапатита. Фазовый и элементный состав образцов после DLP-печати и спекания не претерпевал существенных изменений по сравнению с исходным прокаленным материалом. Прокаленный порошок костного аллотрансплантата пригоден для приготовления фотополимеризуемых суспензий и последующей DLP-печати керамических образцов без ухудшения фазовой и химической стабильности материала. Полученные механические свойства позволяют рассматривать данный аллогенный костный материал в качестве перспективного кандидата для изготовления индивидуализированных имплантатов сложной геометрии.

Ключевые слова: гидроксиапатит, 3D-печать, биокерамика, аллографт, аллоплант, биомедицинское применение, обжиг, керамика

Финансирование: работа выполнена при поддержке гранта Российского научного фонда № 23-15-20042.

Вклад авторов: А. Р. Билялов, С. С. Чугунов — планирование исследования, анализ литературы, интерпретация данных, подготовка рукописи; И. Ш. Ахатов — планирование исследования, интерпретация данных, подготовка рукописи; А. А. Тихонов — планирование исследования, анализ литературы, сбор, анализ, интерпретация данных; О. Р. Шангина — планирование исследования, анализ, интерпретация данных; В. Н. Павлов — планирование исследования; К. В. Данилко — планирование исследования, сбор, анализ, интерпретация данных; М. Ф. Галаутдинов — сбор данных; В. Н. Акбашев — анализ литературы.

✉ **Для корреспонденции:** Азат Ринатович Билялов
ул. Ленина, д. 3, г. Уфа, 450008, Россия; azat.bilyalov@gmail.com

Статья получена: 03.11.2025 **Статья принята к печати:** 29.11.2025 **Опубликована онлайн:** 18.12.2025

DOI: 10.24075/vrgmu.2025.068

The annual number of trauma and orthopedic surgical procedures in Russia exceeded 1.2 million by 2023. The most popular treatment methods include the use of orthopedic bone cement and plastic material for treatment of bone injuries. In the field of orthobiologic procedures, bone grafts and substitutes made up the largest share in 2022 [1].

Autografts are commonly used as effective implants for substitution of bone defects [2], especially in orthopedic and dental surgery. Autografts obtained from the patient, usually from his/her iliac crest, show high biocompatibility, low risk of rejection, and considerable osteogenic potential [3]. When assessing the autograft strengths and weaknesses, allografts turn out to be a promising alternative [4]. Allografts obtained from donors, usually cadaver ones, eliminate the need for additional surgical aggression, thereby reducing the risk of complications. Furthermore, the use of allografts can reduce both surgery and anesthesia time, since there is no need for additional surgical intervention. Moreover, the allograft size and shape can be modified for the implantation area long before the operation, in the preoperative planning phase.

However, allografts are not without drawbacks. Practically, the complexity of creating volumetric bone blocks to match the size of the bone defect is the problem associated with using allografts [5].

The importance of using the DLP ceramic printing technology for medical purposes results from the possibility of creating complex-shaped and functional biocompatible products for implants and reconstructive surgery. DLP provides high processing resolution and precision, which are critical for products made of bioinert or bioactive ceramic materials. This makes it possible to produce porous structures mimicking the bone tissue that contribute to osseointegration and biological function restoration [6].

Traditional ceramic production methods are hampered by the complexity of processing and shaping, while DLP printing allows one to obtain complex geometric shapes without significant expenditure of time and materials. Modern research also reports the importance of optimizing rheological properties of photopolymer suspensions for successful printing and achieving the required mechanical characteristics of products [7].

The ceramic materials used in DLP, such as hydroxyapatite, aluminum oxide, and zirconium oxide, show excellent biocompatibility and bioinertness, which reduce the risk of rejection and inflammatory responses in patients. The technology allows for control of the surface microstructure, which improves the implant adhesion to tissues [6].

The DLP printing works well with other additive production and post-processing methods, thereby expanding the possibilities for the creation of multifunctional and composite materials for medical use [8].

In this study we assess applicability of the digital light processing (DLP)-based additive production method to the hydroxyapatite material obtained from cortical bones of the cadaver bone allograft. As far as we know, no studies devoted specifically to additive production of ceramic products using human bone allografts have been presented in the literature to date.

The material used in this study represents the commercially available medical bone allograft in the form of blocks (Alloplant® allografts for surgery according to MS 9398-001-04537642-2011; registration certificate for a medical product FSR 2011/12012; manufacturer — Bashkir State Medical University, Russia). This commercially available material is widely used in medical practice; more than 2,000 orthopedic surgeries are performed in medical clinics every year.

The study was initiated in response to requests from practicing surgeons concerning the development of advanced technologies for production of allografts. The main purpose of using this allograft material in 3D printing is to achieve high precision of geometry parameters with deviations within hundreds microns, allowing for adaptation of products to the irregularly shaped bone defects while maintaining high biomedical properties.

The study aimed to assess applicability of the digital light processing (DLP)-based additive production technology for forming high-precision complex-shaped implants made of the bone allograft-derived material.

METHODS

Allograft material processing and photopolymerizable suspension preparation

The cadaver bone material is through a number of chemical treatment and radiation sterilization procedures to remove immunogenic components and induce lysis of membrane tissues; collagen and some elements of the amorphous bone matrix are preserved [9]. The study design is presented in Fig. 1.

The bone blocks sized 0.5–6 cm were calcined in the Kittec CLL15 laboratory kiln (Kittec, Germany) at a temperature of 900 °C for 5 h in order to remove organic content. There were yellowish and grayish deposits on the surface of approximately 15% of the calcined blocks. Both clean calcined blocks and blocks with deposits were analyzed using the Jeol JSM-6390LV scanning electron microscope (JEOL, Japan) equipped with the energy-dispersive X-ray analyzer (EX-230 BU).

After calcination the allograft material was through the two-stage grinding procedure involving the zirconium grinding cups and zirconium balls in the Retsch PM400 planetary ball mill (Retsch, Germany). Stage 1 aimed to grind the allograft blocks into the millimeter-sized powder. Stage 2 aimed to grind into particles sized 1–5 μm. Such grinding included wet grinding in isopropanol (IPA). Then the ground material was dried in the Binder ED56 drying oven (Binder GmbH, Germany) at 115 °C for 2 h to eliminate the remaining IPA.

After stage 1 of grinding the powder fraction was obtained using the laboratory sieves with the mesh size of 400 μm and 315 μm. Sample A consisted of the 315–400 μm powder fraction. Sample B was obtained from the resulting powder after stage 2 of grinding.

The micron-sized allograft powder was mixed with the Dysperbyk-180 dispersing additive (BYK GmbH, Germany) at a mass concentration of 2% in the Retsch PM400 planetary ball mill using the 8-mm zirconium balls with the speed of 200 rpm for 1 h. To produce a photopolymerizable suspension, the CB2-DLP-GM/2 organic binder (Vundertech LLC, Russia) was mixed with the E104 dye at a mass concentration of 0.24% and then added to the dispersed allograft powder to achieve the powder load with the mass concentration of 68.9%, which corresponded to the concentration of 42.6% v/v. The dye was included to minimize light scattering by ceramic particles during 3D printing. Finally, the suspension was homogenized in the Retsch PM400 planetary ball mill using the 20-mm zirconium balls with the speed of 200 rpm for 5 h.

Tesing the photopolymerizable suspension and 3D printing operations

All the tests involving the photopolymerizable suspension were conducted using the Creality Mage Pro 8K DLP 3D printer (Creality, China).

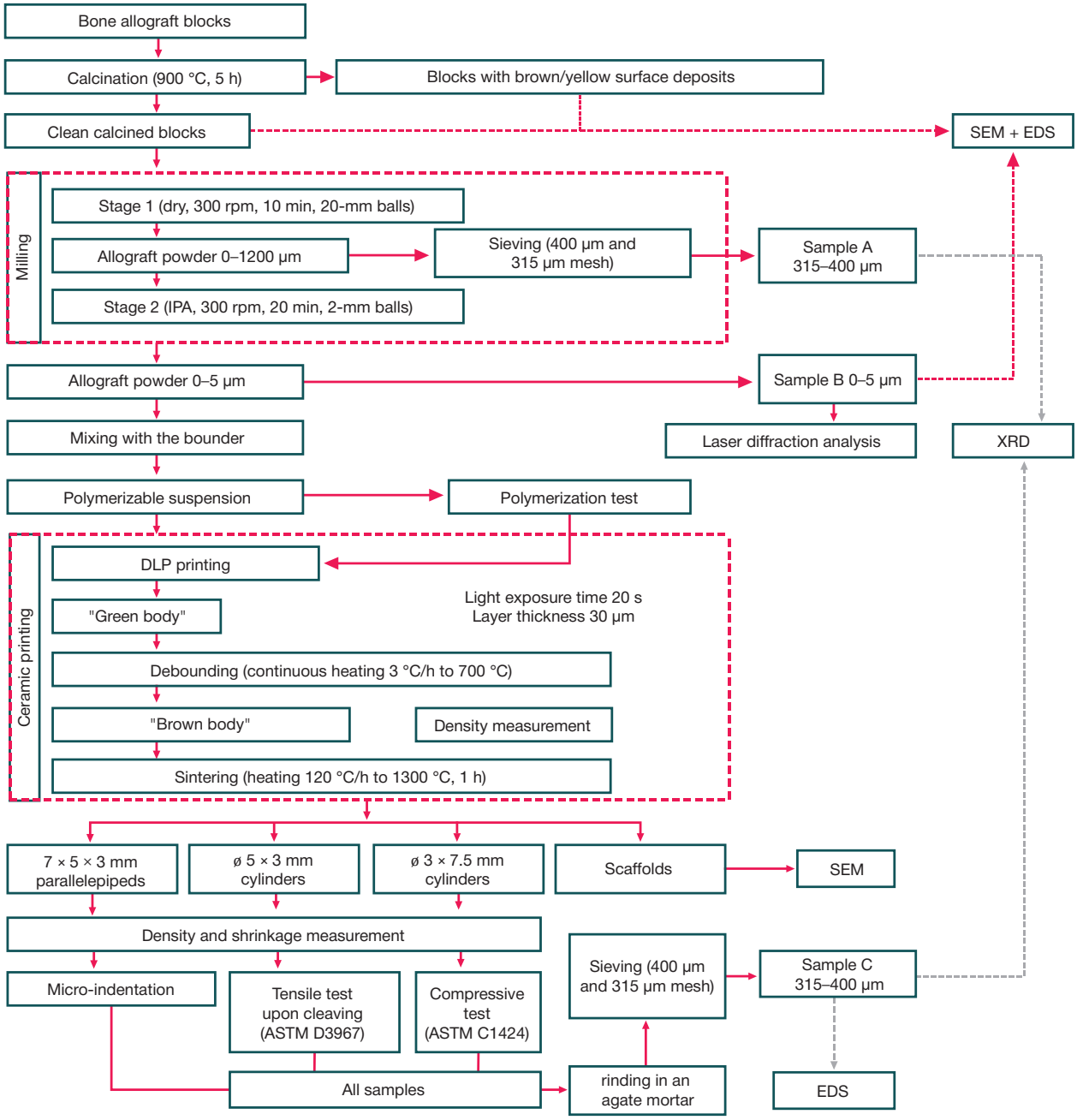

Fig 1. Study design

First, the syspension polymerization effectiveness was assessed. The square objects sized 1 × 1 cm were polymerized at different light energy of 0.12, 0.2, 0.24, 0.8, and 16 J/cm^2, which corresponded to the exposure time of 15, 25, 30, 100, and 2000 s, respectively. In each case, the 2 mm-thick suspension layer was placed in the printer bath, and the experiment was repeated four times. After polymerization the polymerized layer thickness was measured using the Interapid thickness gauge (Schut, Switzerland) with an accuracy of 0.001 mm. Such evaluation yielded two important results: a) confirmation that the allograft-based suspension was suitable for DLP printing; b) determination of the relationship between light energy and polymerization depth.

Optimal 3D printing parameters were determined based on this relationship: exposure time of 20 s and layer thickness of 30 μm. 3D printing was conducted in two series. The first series involved production of the cylinders sized 3–7.5 mm for mechanical compressive testing (ASTM C1424) [10] and X-ray diffraction analysis (ISO 10993-14) [11] and parallelepipeds sized 7 × 5 × 3 mm for measurement of the density, shrinkage during sintering, porosity, Vickers hardness (ISO 10993-14).

The second series involved evaluation of the possibility of printing complex ceramic structures in the form of a mesh or scaffold. After 3D printing all the objects were subjected to thermal debounding in the Kittec CLL15 kiln through heating to 700 °C with the rate of 3 °C/h in air. The object size was measured using the Topex 31C628 caliper (Group Topex, Poland) with an accuracy of 0.02 mm, while mass measurement was performed using the AND HR250-AZG laboratory scales (AD Company, Japan) with an accuracy of 0.001 g. This measurement allowed us to accurately estimate the samples' density and porosity at the non-sintered product (raw material) stage.

After the bounder removal (debounding) the samples showed porosity of 58% and were characterized as loosely consolidated and mechanically weak. These were sintered in

the Kittec CLL15 kiln in air at a temperature of 1300 °C with the heating rate of 120 °C/h and subsequently conditioned for 1 h.

After the end of testing physical and mechanical characteristics of the sintered allograft material the previously fractioned samples, cylinders and parallelepipeds, were grinded in the agate mortar and sieved to obtain the 315–400 μm powdery fraction. Sample C was collected from the resulting powder.

Laboratory assessment of the material properties

Assessment of the non-sintered allograft material

The energy-dispersive spectroscopy was used to assess chemical composition of the calcined allograft blocks, specifically of the clean fragments and yellowish and grayish surface deposits. This method was also used for Sample B to assess chemical composition of the target powdery material for 3D printing. It was expected that the Sample B composition would reflect the effects of calcination and grinding, including potential chemical activation or degradation of chemical compounds. The powdery sample was evenly distributed over the area of 1 × 1 cm of the sample holder in the scanning electron microscope (SEM) and examined at two different sites using the voltage of 20 kV and the exposure time of 120 s.

The particle size distribution in Sample B was assessed using the Fritsch Analysette 22 NanoTec laser particle sizer (Fritsch GmbH, Idar-Oberstein, Germany) to make sure that most particles in the powder were smaller than 10 μm, in accordance with the requirements of the digital light processing (DLP) technique.

Assessment of physical and mechanical properties of the additively manufactured sintered allograft material

The density and porosity of green, calcined, and sintered objects were calculated based on the measured size and mass. Measurement was performed for each object individually. The size was measured using the Topex 31C628 caliper, while mass measurement was performed using the AND HR250-AZG scales. The relative density was calculated based on the hydroxyapatite theoretical density (3.16 g/cm^3).

The coefficients of shrinkage due to thermal sintering were calculated by assessing changes in size between the object's green and sintered states. It is important to note that the shrinkage coefficients in the X, Y, and Z directions were different due to the 3D printing anisotropic nature.

Hardness of the parallelepiped objects was assessed using the Nanovea PB1000 mechanical tester (Nanovea, USA) equipped with the Vickers hardness tester. The compressive and tensile tests upon cleaving were performed using the Instron 5969 dual column testing system (Instron, USA). Compressive tests were compliant with the ASTM C1424 standards, and the test samples were cylinders sized 3–7.5 mm. These samples were produced in accordance with the X2 chapter of the ASTM C1424 test standard [10], but these were proportionally reduced in size by 40%. Evolution of the two-dimentional deformation field during loading was recorded using the Vic-3D Digital Image Correlation (DIC) measurement system (Correlated Solutions Inc., USA).

Parameters of the sintered allograft material tension were obtained from the tensile tests upon cleaving conducted in accordance with ASTM D3967.

The additively manufactured sintered scaffold was tested for potential structural artifacts using the Helios G4 PFIB ThermoFisher Scientific scanning electron microscope (ThermoFisher Scientific, USA).

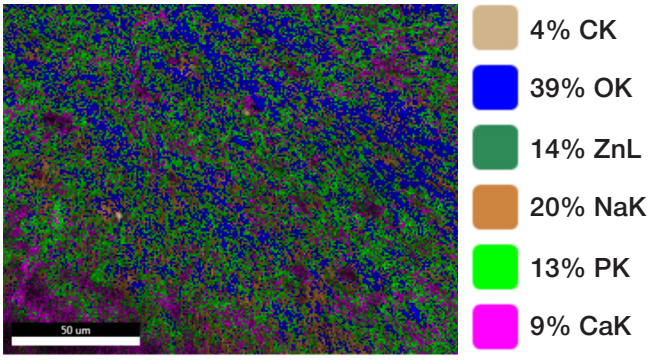

Fig. 2. Results of the EDS analysis of colored deposits on the surface of calcined allografts: distribution of chemical elements across the yellowish deposit area, several colors of some compounds correspond to the same set of chemical components appearing in different orders in the EDS results, for example Ca/P/O/Na/Zn or Ca/P/O/Zn/Na

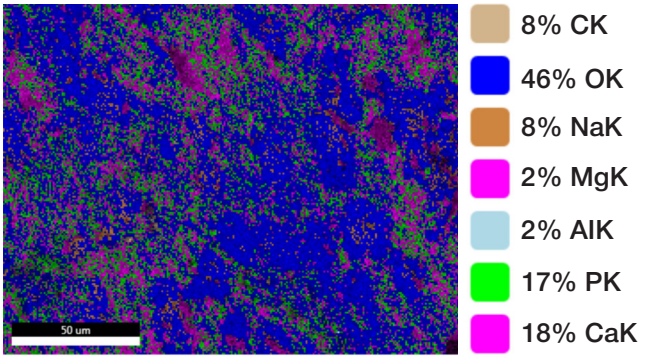

Fig. 3. Results of the EDS analysis of the surface of the calcined allograft with no identifiable deposits: distribution of chemical elements across the allograft area. Several colors of some compounds correspond to the same set of chemical components appearing in different orders in the EDS results, for example Ca/P/O/C or Ca/C/P/O

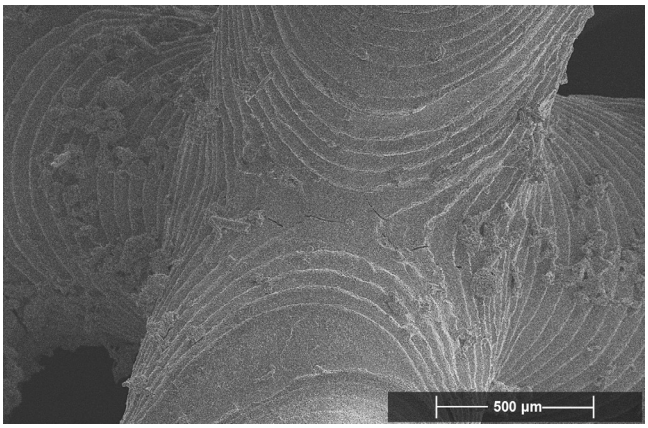

Fig. 4. Allograft-derived 3D-printed complex-shaped sintered scaffold. Convex and concave areas of the object and the layered structure are visible; microcracks in the layered structure of the object emerged during heat treatment

Assessment of evolution of the allograft phase in additive manufacturing processes

Assessment of the material phase evolution at various stages of the production process was performed for samples A, B, and C using the Guinier camera coupled with the Huber G670 X-ray diffractometer (Huber Diffraktionstechnik GmbH Co. KG, Germany). Powdery samples were applied on the Mylar film using acetone before transfer for testing. Measurement was performed using the Ge (111) curved monochromator and the image plate detector using CoKα1 (λ = 1.78892 Å). The assessed 2θ range was 4–100° with the 0.01° angular step.

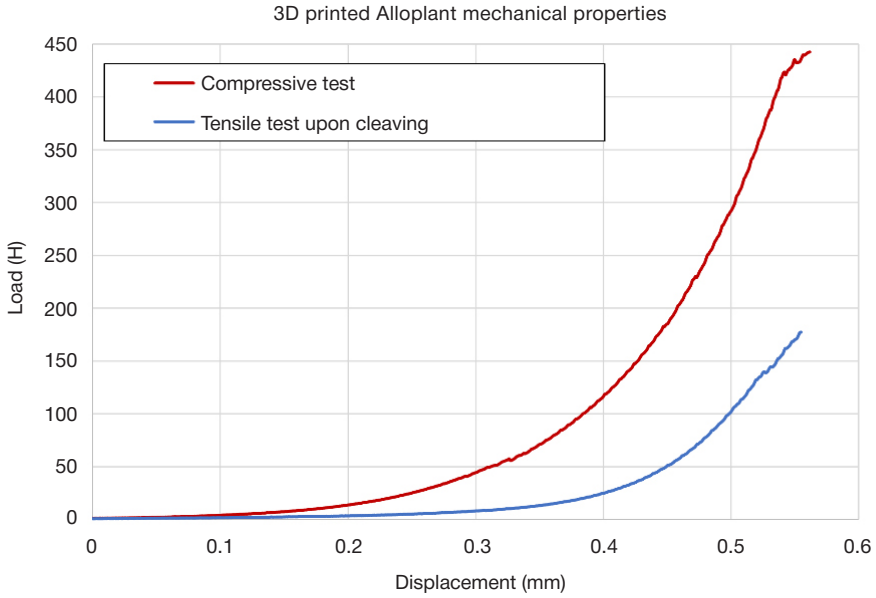

Fig. 5. Mechanical behavior of the 3D-printed allograft material sintered at 1300 — during the mechanical compressive test (6 samples) and tensile test upon cleaving (6 samples)

The analysis of the X-ray diffraction (XRD) testing results was conducted using the ICDD PDF-2 database (The International Centre for Diffraction Data Powder Diffraction File-2). The XRD testing results for samples A, B, and C were compared to assess the impact of the material grinding and heat treatment.

RESULTS

Assessment of the non-sintered allograft material

Calcination of the allograft bulk samples eliminates residual organic content and ethanol from the allograft material yielding the dry, brittle ceramic matrix. The mass loss during calcination was 41.9%.

In our analysis of the processed allograft bulk samples, about 15% of bone blocks showed visible surface deposits. These deposits included the zinc-rich yellowish substances and the grayish matter containing a considerable amount of carbon. Some yellowish deposits also showed traces of the grayish matter. Other samples looked clean and white, with no visible signs of deposits.

The analysis of the deposit chemical composition by EDS revealed high zinc concentrations, probably in the form of yellow-brown hopeite crystals, in the yellowish deposits (Fig. 2). The analysis revealed the calcium, phosphorus, oxygen, sodium and zinc atoms, which together accounted for up to 82% of the area examined. The remaining 18% included similar chemical components along with additional carbon atoms, possibly indicating a limited amount of soot formed from the decomposition of organic matter.

Significant amounts of carbon, probably in the form of soot, were found in the greyish deposits. The EDS results showed that there were no detectable calcium atoms in these grayish areas, and 84% of the area analyzed also contained no phosphorus.

The EDS analysis of visually clean calcined allograft samples revealed atoms of calcium, phosphorus, and oxygen in all the areas examined. Up to 93% of these areas were still covered with a thin layer of carbon deposits, while 27% contained sodium atoms (Fig. 3). It was impossible to accurately determine the Ca/P ratio based on the EDS data on the calcined sample surfaces, since during thermal decomposition the organic matter was likely to diffuse through the porous structure of the inorganic matrix causing uneven distribution of elements across the surface.

The scanning electron microscopy (SEM) has shown that the calcined allograft consists of the tightly packed grains of calcium phosphate ceramics sized 130 nm–2.2 μm. The grains have a rounded morphology typical for sintered ceramics.

After calcination the allograft organic content decomposed, which increased fragility and made grinding easier. At the first stage the calcined bone was ground to powder with the particle size below 1.2 mm and sieved through the 1200 μm sieve. At the second stage powder with the particle size 0–5 μm was obtained. According to the laser diffractometry results, the particle size is 300 nm–5 μm, the average value is 2.57 μm. The secondary peak of the distribution (5–25 μm) is due to agglomerates of small particles, which is confirmed by SEM. Such agglomerates do not interfere with DLP processes, as these are destroyed during the suspension preparation.

Assessment of physical and mechanical properties of the additively manufactured sintered allograft material

Based on polymerization tests of the photopolymerizable suspension we determined the relationship between light energy and polymerization depth. According to the method by Jacobs [12], the critical energy required for effective polymerization is Ec = 3.51 mJ/cm^2, which is in line with the capabilities of the 3D printer used. The minimum exposure time ensuring polymerization was determined as 15 s (layer thickness 122 μm), but such samples were soft and unstable. With the 20 s exposure, solid and durable “green bodies” without defects were produced. Simple-shaped objects and scaffolds were successfully printed by the DLP method, cleared of binder, and sintered.

The scaffold was examined by SEM (Fig. 4). The layered structure was clearly visible. During heat treatment microcracks with the holes sized about 10–15 μm emerged in the contact zones of the protruding structures, which suggests the need to optimize sintering. Internal surfaces of the cracks contained the densely packed grains sized 5–10 μm, while the source powder had the 0.3–5 μm grains, which suggests rearrangement and growth of grains during sintering.

The lack of nanoporous voids in the corners of conjugated grains, typical for high-temperature sintering, is noteworthy. The material contains intergranular microcracks, which can form a porous system in the absence of nanopores. With the relative density of 82%, the expected porosity of 19% is consistent with the observations. Porosity results from intergranular microcracks and large voids between clusters of grains, which is typical for low-density materials.

The allograft compaction during sintering resulted in reduction of the linear dimensions and geometric features. The average linear shrinkage of the allograft was 24%. Such anisotropic shrinkage typical for 3D printing can be associated with uneven application of the source material both inside and outside the layer formation plane.

The EDS results obtained for Sample C give an idea about the ratio of calcium and phosphorus (Ca/P), since these cover the data on both surface and bulk of material. The EDS analysis shows that the main sintered allograft material components are calcium (Ca), phosphorus (P), and oxygen (O), as well as trace amounts of sodium (Na), magnesium (Mg), strontium (Sr), aluminum (Al), and potassium (K).

The Ca/P ratio varied between 1.6 and 1.7 in the eight samples tested.

The results of compressive and tensile tests upon cleaving are provided in Fig. 5. The sintered allograft material compressive strength varied between 50 and 100 MPa, with the average value of 76 MPa. The tensile strength obtained from the tensile test upon cleaving varied between 4 and 23 MPa, with the average value of 12 MPa. Furthermore, the Young's modulus turned out to be between 2.9 and 3.3 GPa.

The sintered allograft material Vickers hardness varied between 0.3 and 0.8 GPa.

Such a high local hardness value can be associated with the ZrO_2 incorporation resulting from grinding. Except for this outlier, the average Vickers hardness was approximately 0.6 GPa.

Assessment of the allograft phase evolution due to milling and additive production processes

The X-ray diffraction (XRD) analysis results for samples A, B, and C fit closely with the control peaks for the "[9–432] Hydroxyapatite" record of the ICDD PDF-2 database. All the test samples were calcined at 900 °C before XRD analysis, which reflects the effects of such treatment. Small amorphous phase amounts were found in Sample A and Sample B, which was indicated by wider peaks and small deviations from the baseline. Sample C, on the contrary, showed narrower and sharper peaks, which suggests the reduced amorphous phase content. Moreover, new peaks corresponding to CaO ($2\theta \approx 43°$) and ZrO_2 ($2\theta \approx 34°$) were identified in Sample C. The presence of CaO inclusions can be explained by mechanical activation and potential degradation of hydroxyapatite and amorphous calcium phosphate compounds. The ZrO_2 peaks are related to the zirconium dioxide inclusions that contaminated the allograft material at the second stage of milling.

DISCUSSION

The allograft material obtained from cadaver human cortical bones showed potential for successful use in the digital light processing (DLP)-based additive procedure. We have found no studies focused on using bone allografts for 3D printing in the scientific literature. We have shown that the bone allograft-based material can be effectively used together with the additive production methods showing the behavior similar to that of synthetic hydroxyapatite during 3D printing.

The printing and heat treatment protocols optimized for synthetic calcium phosphate ceramics did not ensure the required properties of the bone-derived allograft. The sign of this were cracks in the sintered samples caused by low density of brown bodies and suboptimal sintering. The density can be increased by increasing the amount of powder in the photopolymerizable suspension. Optimization of sintering will require a series of parametric tests and laboratory analysis of material properties.

Despite the fact that the process of producing the samples manufactured by the additive method from the allograft was not optimized, it made it possible to obtain the relatively high sintering density on a microscale, which suggests the potential for further improvement. It is noteworthy that there were no voids in the corners of conjugated grains, and the natural chemical inclusions in the material structure, such as sodium (Na), magnesium (Mg), strontium (Sr), aluminum (Al), and potassium (K), were preserved in the amounts typical for human bones. These factors indicate that the allograft properties are superior to that of synthetic alternatives.

The milling operations contributed to effective homogenization of the allograft chemical composition. However, due to low powder filling coefficient of the source material, the "brown body" baseline density was not enough, which resulted in the unnecessary stress and insufficient compaction during thermal sintering. As a result, intergranular microcracks and large intergranular voids emerged, which contributed to the sintered material porosity in 15.8%. The calcium phosphate crystals in the intact bone represent the plate-shaped particles sized 40 × 3 × 7.5 nm intertwined with the collagen fibers [12]. The lack of such nanoplates in the calcined sample indicates sintering and transformation of those into roundish grains during calcination.

No significant changes in the material phases or chemical composition were observed throughout the production process. The commercially available human bone allograft contains about 60–70% minerals and 30–40% organic components (by mass) [13–15]. Thorough analysis confirmed the calcium-deficient nature of the bone-derived mineral with the average calcium to phosphorus ratio (Ca/P) of 1.65. The calcium phosphate ceramics resorb faster as the Ca/P ratio decreases. That is why it is expected that bioresorption of allograft materials will proceed faster than that of synthetic hydroxyapatite. This ratio is consistent with expectations for the calcium-deficient hydroxyapatite phase, confirmed by the X-ray diffraction (XRD) results [16]. Some studies report that the human bone average Ca/P ratio is about 1.67 [17], while according to the results of other studies [18], the bone mineral usually has the Ca/P ratio below 1.67 due to calcium deficiency.

The sintered material mechanical properties are critical for determination of its overall strength and hardness, especially considering the non-oprimized material microstructure. Therefore, the material properties can be improved through optimization of processing and production technologies.

CONCLUSIONS

The allograft material used in this study was obtained from the cadaver human cortical bone tissue. This material was calcined and then ground into the micron-sized powder to produce a photopolymerizable suspension and to be later used for the DLP-based additive production. The results confirmed high compatibility of the allograft material with the additive production technologies. Polymerization tests and 3D printing operations demonstrated stability of the bone allograft-derived material at every stage of additive production. Further research

is necessary to clarify the characteristics of the additively manufactured allograft implants and compare these with synthetic analogues. This includes optimization of the additive production process preparation stages and assessment of their potential aimed to regulate osteoinduction, osteoconduction, and mechanical stability both in vitro and in vivo.

References

1. GlobalData Plc, United States (US) Orthopedic Procedures Count By Segments And Forecast To 2030, GlobalData Plc, John Carpenter House, John Carpenter Street, London, EC4Y 0AN, UK, 2023. Available from: https://www.globaldata.com/store/report/usa-orthopedic-procedures-analysis/#:~:text=US%20Orthopedic%20Market%20Report%20Overview,US%20was%2018%2C577%2C953%20in%202022.
2. Rogers GF, Greene AK, Autogenous bone graft: basic science and clinical implications, J Craniofac Surg. 2012; 23: 323–7. Available from: https://doi.org/10.1097/SCS.0b013e318241dcba
3. Dutta SR, Passi D, Singh P, Bhuibhar A, Ceramic and non-ceramic hydroxyapatite as a bone graft material: a brief review. Ir J Med Sci. 1971; 184 (2015): 101–06. Available from: https://doi.org/10.1007/s11845-014-1199-8.
4. Yang C, Zhuo W, Li Q, Huang C, Yan H, Jin D, Preliminary outcomes of allograft and hydroxyapatite as substitutes for autograft in anterior cervical discectomy and fusion with self-locking standalone cages. J Orthop Surg. 2021; 16: 123. Available from: https://doi.org/10.1186/s13018-021-02257-0.
5. Rasch A, Naujokat H, Wang F, Seekamp A, Fuchs S, Klüter T, Evaluation of bone allograft processing methods: Impact on decellularization efficacy, biocompatibility and mesenchymal stem cell functionality. PLOS ONE. 2019; 14: e0218404. Available from: https://doi.org/10.1371/journal.pone.0218404.
6. Buj-Corral I, Tejo-Otero A. 3D Printing of Bioinert Oxide Ceramics for Medical Applications. J Funct Biomater. 2022; 13 (3): 155. DOI: 10.3390/jfb13030155. PMID: 36135590; PMCID: PMC9505679. Available from: https://doi.org/10.3390/jfb13030155.
7. Thakur N, Carretta M, Komissarenko D, Blugan G. Advancements in DLP 3D printing: High strength alumina toughened zirconia ceramics for biomedical applications. Open Ceramics. 2024; 18: 100601. Available from: https://doi.org/10.1016/j.oceram.2024.100601.
8. Sadaf Bashir Khan, Syed Irfan, Zhengjun Zhang, Weifeng Yuan. ACS Applied Bio Materials. 2025; 8 (8): 6470–525. Available from: https://doi.org/10.1021/acsabm.4c01923.
9. Muldashev ER, Muslimov SA, Vyalkov VA, Galimova VU, Nigmatullin RT, Salikhov AY, et al. Biomaterial alloplant dlja regenerativnoj hirurgii, RU2189257C1. 2002.
10. American Society for Testing and Materials, ASTM C1424 -Standard Test MEthod for Monolithic Compressive Strength of Advanced Ceramics at Ambient Temperature. 2004.
11. International Organization for Standardization, ISO 10993-14:2001(E): Biological evaluation of medical devices — Part 14: Identification and quantification of degradation products from ceramics. 2001.
12. Jacobs PF. Fundamentals of Stereolithography. 1992.
13. Dey P. Bone Mineralisation. In: Churchill DG, Dutour Sikirić M, Čolović B, Füredi H. Milhofer, editors. Contemp Top Phosphorus Biol Mater. IntechOpen. 2020. Available from: https://doi.org/10.5772/intechopen.92065.
14. Pietrzak WS, Woodell-May J, The Composition of Human Cortical Allograft Bone Derived from FDA/AATB-Screened Donors. J Craniofac Surg. 2005; 16: 579–85. Available from: https://doi.org/10.1097/01.SCS.0000159086.44801.C7.
15. Wang W, Yeung KWK, Bone grafts and biomaterials substitutes for bone defect repair: A review. Bioact Mater. 2017; 2: 224–47. Available from: https://doi.org/10.1016/j.bioactmat.2017.05.007.
16. Kuhn LT, Grynpas MD, Rey CC, Wu Y, Ackerman JL, Glimcher MJ. A Comparison of the Physical and Chemical Differences Between Cancellous and Cortical Bovine Bone Mineral at Two Ages. Calcif Tissue Int. 2008; 83: 146–54. Available from: https://doi.org/10.1007/s00223-008-9164-z.
17. Ishikawa K, Ducheyne P, Radin S, Determination of the Ca/P ratio in calcium-deficient hydroxyapatite using X-ray diffraction analysis. J Mater Sci Mater Med. 1993; 4: 165–8. Available from: https://doi.org/10.1007/BF00120386.
18. Gotoh Y, Hiraiwa K, Nagayama M. In vitro mineralization of osteoblastic cells derived from human bone. Bone Miner. 1990; 8: 239–50. Available from: https://doi.org/10.1016/0169-6009(90)90109-s.

Литература

1. GlobalData Plc, United States (US) Orthopedic Procedures Count By Segments And Forecast To 2030, GlobalData Plc, John Carpenter House, John Carpenter Street, London, EC4Y 0AN, UK, 2023. Available from: https://www.globaldata.com/store/report/usa-orthopedic-procedures-analysis/#:~:text=US%20Orthopedic%20Market%20Report%20Overview,US%20was%2018%2C577%2C953%20in%202022.
2. Rogers GF, Greene AK, Autogenous bone graft: basic science and clinical implications, J Craniofac Surg. 2012; 23: 323–7. Available from: https://doi.org/10.1097/SCS.0b013e318241dcba
3. Dutta SR, Passi D, Singh P, Bhuibhar A, Ceramic and non-ceramic hydroxyapatite as a bone graft material: a brief review. Ir J Med Sci. 1971; 184 (2015): 101–06. Available from: https://doi.org/10.1007/s11845-014-1199-8.
4. Yang C, Zhuo W, Li Q, Huang C, Yan H, Jin D, Preliminary outcomes of allograft and hydroxyapatite as substitutes for autograft in anterior cervical discectomy and fusion with self-locking standalone cages. J Orthop Surg. 2021; 16: 123. Available from: https://doi.org/10.1186/s13018-021-02257-0.
5. Rasch A, Naujokat H, Wang F, Seekamp A, Fuchs S, Klüter T, Evaluation of bone allograft processing methods: Impact on decellularization efficacy, biocompatibility and mesenchymal stem cell functionality. PLOS ONE. 2019; 14: e0218404. Available from: https://doi.org/10.1371/journal.pone.0218404.
6. Buj-Corral I, Tejo-Otero A. 3D Printing of Bioinert Oxide Ceramics for Medical Applications. J Funct Biomater. 2022; 13 (3): 155. DOI: 10.3390/jfb13030155. PMID: 36135590; PMCID: PMC9505679. Available from: https://doi.org/10.3390/jfb13030155.
7. Thakur N, Carretta M, Komissarenko D, Blugan G. Advancements in DLP 3D printing: High strength alumina toughened zirconia ceramics for biomedical applications. Open Ceramics. 2024; 18: 100601. Available from: https://doi.org/10.1016/j.oceram.2024.100601.
8. Sadaf Bashir Khan, Syed Irfan, Zhengjun Zhang, Weifeng Yuan. ACS Applied Bio Materials. 2025; 8 (8): 6470–525. Available from: https://doi.org/10.1021/acsabm.4c01923.
9. Muldashev ER, Muslimov SA, Vyalkov VA, Galimova VU, Nigmatullin RT, Salikhov AY, et al. Biomaterial alloplant dlja regenerativnoj hirurgii, RU2189257C1. 2002.
10. American Society for Testing and Materials, ASTM C1424 -Standard Test MEthod for Monolithic Compressive Strength of Advanced Ceramics at Ambient Temperature. 2004.
11. International Organization for Standardization, ISO 10993-14:2001(E): Biological evaluation of medical devices — Part 14: Identification and quantification of degradation products from ceramics. 2001.
12. Jacobs PF. Fundamentals of Stereolithography. 1992.
13. Dey P. Bone Mineralisation. In: Churchill DG, Dutour Sikirić M, Čolović B, Füredi H. Milhofer, editors. Contemp Top Phosphorus Biol Mater. IntechOpen. 2020. Available from: https://doi.org/10.5772/

intechopen.92065.
14. Pietrzak WS, Woodell-May J, The Composition of Human Cortical Allograft Bone Derived from FDA/AATB-Screened Donors. J Craniofac Surg. 2005; 16: 579–85. Available from: https://doi.org/10.1097/01.SCS.0000159086.44801.C7.
15. Wang W, Yeung KWK, Bone grafts and biomaterials substitutes for bone defect repair: A review. Bioact Mater. 2017; 2: 224–47. Available from: https://doi.org/10.1016/j.bioactmat.2017.05.007.
16. Kuhn LT, Grynpas MD, Rey CC, Wu Y, Ackerman JL, Glimcher MJ. A Comparison of the Physical and Chemical Differences Between Cancellous and Cortical Bovine Bone Mineral at Two Ages. Calcif Tissue Int. 2008; 83: 146–54. Available from: https://doi.org/10.1007/s00223-008-9164-z.
17. Ishikawa K, Ducheyne P, Radin S, Determination of the Ca/P ratio in calcium-deficient hydroxyapatite using X-ray diffraction analysis. J Mater Sci Mater Med. 1993; 4: 165–8. Available from: https://doi.org/10.1007/BF00120386.
18. Gotoh Y, Hiraiwa K, Nagayama M. In vitro mineralization of osteoblastic cells derived from human bone. Bone Miner. 1990; 8: 239–50. Available from: https://doi.org/10.1016/0169-6009(90)90109-s.